

Efficient Partial Element Calculation and the Extension to Cylindrical Elements for the PEEC Method

A. Müsing and J. W. Kolar
Power Electronic Systems Laboratory, ETH Zürich
CH-8092 Zürich, Switzerland

Abstract- For various electrical interconnect and EMC problems, the Partial Element Equivalent Circuit (PEEC) method has proven to be a valid and fast solution method of the electrical field integral equation in the time as well as the frequency domain. Therefore, PEEC has become a multi-purpose full-wave simulation method, especially suited for the solution of combined circuit and EM problems, as found on printed circuit board layouts, power electronics devices or EMC filters. Recent research introduced various extensions to the basic PEEC approach, for example a non-orthogonal cell geometry formulation. This work presents a fast, flexible and accurate computational method for determining the matrix entries of partial inductances and the coefficients of potential for general non-orthogonal PEEC cell geometries. The presented computation method utilizes analytical filament formulas to reduce the integration order and therefore to reduce computation time. The validity, accuracy and speed of the proposed method is compared with a standard integration routine on example cell geometries where the numeric results of the new method show improved accuracy, coming along with reduced computation time. Furthermore, this work shows an extension to cylindrical elements which is consistent with classical PEEC models, using the proposed integration routines for the partial element calculations.

I. INTRODUCTION

The increasing performance of power electronic circuits is obtained mainly by increasing the switching frequency and the circuit complexity. This fact is true on the microscopic scale for on-chip VLSI design, as well as for macroscopic power electronics circuits. Due to the resulting fast voltage and current transients, the modeling of electric interconnects and the analysis of their electromagnetic behaviour is gaining in importance.

For the solution of mixed EM problems, the Partial Element Equivalent Circuit (PEEC) method [1] has become a very popular approach. The method is based on a circuit interpretation of the Electric Field Integral Equation (EFIE). Unlike the method of moments, PEEC is a full-spectrum method valid from DC to a maximum frequency determined by the meshing. Further extensions, especially the introduction of time retardation [2], dielectric cells [3] and the formulation with non-orthogonal cell geometries [4] have made PEEC a multi-purpose electromagnetic solver. A PEEC simulation is mainly performed in the following steps:

- 1) Geometry discretization of the layout and placement of external components such as current and voltages sources or load impedances,
- 2) fill-in of partial inductance matrices L_p and partial coefficients of potential matrices P_n and the setup of the matrix equation system, typically in modified nodal analysis (MNA) formulation,
- 3) time domain or frequency domain solution of the system matrix equation in

a SPICE-like solver and 4) postprocessing or graphical visualization of the simulation results.

The bottlenecks of simulation effort are both, matrix fill-in and the subsequent solution of the equation systems, which limit the maximum problem size to 10^4 - 10^5 unknown variables, namely the node voltages and currents. The partial element computation is the limiting factor in particular for non-orthogonal cell geometries, since fast analytical formulas are not directly applicable. Hence, a cumbersome multidimensional integration must be performed numerically for every entry in the inductance matrix L_p and the coefficient of potential matrix P_n . Furthermore, the obtained accuracy of partial elements has direct influence on the stability of time-domain models [5] and a fast computation with high precision is desirable.

This work is introducing a new integration method using analytic solutions for the Neumann integral along straight and arbitrarily aligned current filaments [6] to accelerate the calculation of non-orthogonal partial elements. This technique can be applied to the mutual couplings between the PEEC cells as well as the self-terms represented by the diagonal elements of the L_p and P_n matrices.

The paper is organized as follows: First, a short introduction on the simulation method is given, followed by a derivation of the accelerated partial element computation using analytic filament formulas and its application on newly introduced cylindrical PEEC elements. Then, the proposed method is exemplified on simple and comprehensible numeric examples. Finally, a discussion and outlook concludes this work.

II. NON-ORTHOGONAL PEEC FORMULATION

The classical PEEC method is derived from the equation for the total electric field at a point written as

$$\mathbf{E}_i(\mathbf{r}, t) = \frac{\mathbf{J}(\mathbf{r}, t)}{\sigma} + \frac{\partial \mathbf{A}(\mathbf{r}, t)}{\partial t} + \nabla \phi(\mathbf{r}, t) \quad (1)$$

where \mathbf{E}_i is an incident electric field, \mathbf{J} is a current density, \mathbf{A} is the magnetic vector potential, and ϕ is the scalar electric potential. By using the definitions of the scalar and vector potentials, the current- and charge densities are discretized by defining pulse basis functions for the conductors and dielectric materials. Pulse functions are also used for the weighting functions resulting in a Galerkin type solution. By defining a suitable inner product, a weighted volume integral over the cells, the field equation (1) can be interpreted as Kirchhoff's voltage law over a PEEC cell consisting of partial self inductances between the

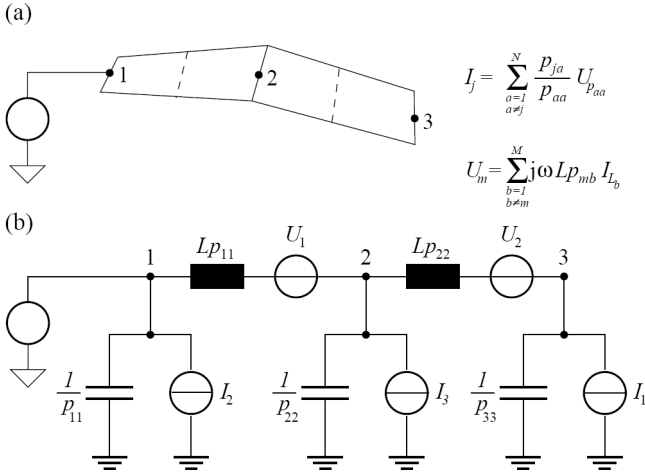


Figure 1. Two non-orthogonal conductor cells (a) and their corresponding equivalent circuit (b).

nodes and partial mutual inductances representing the magnetic field coupling in the equivalent circuit. The partial inductances, shown as Lp_{ij} in Fig. 1, are defined as

$$Lp_{ij} = \frac{\mu}{4\pi} \frac{1}{a_i a_j} \iint_{v_i v_j} \frac{1}{|\mathbf{r}_i - \mathbf{r}_j|} dv_i dv_j. \quad (2)$$

Fig. 1 also shows the node capacitances which are related to the diagonal coefficients of potential p_{ii} while ratios consisting of p_{ij}/p_{ii} are modeled with controlled current sources in the PEEC circuit. The coefficients of potentials are computed as

$$p_{ij} = \frac{1}{4\pi\epsilon_0} \frac{1}{S_i S_j} \iint_{S_i S_j} \frac{1}{|\mathbf{r}_i - \mathbf{r}_j|} dS_i dS_j. \quad (3)$$

Introducing a local non-orthogonal coordinate system (a, b, c, a', b', c'), see Fig. 2, the general self and mutual partial inductances can be extended to a non-orthogonal formulation as detailed in [4]. Then, the inductances are computed as

$$Lp_{aa'} = \mu \iiint_a \iiint_b \iiint_{c'} \hat{\mathbf{a}} \cdot \hat{\mathbf{a}}' \left| \frac{\partial \mathbf{r}}{\partial a} \right| \left| \frac{\partial \mathbf{r}'}{\partial a'} \right| G(\mathbf{r}, \mathbf{r}') dv dv' \quad (4)$$

and likewise, the coefficients of potential are given by

$$Pn_{aa'} = \frac{1}{\epsilon} \iiint_a \iiint_{a'} G(\mathbf{r}, \mathbf{r}') dA dA'. \quad (5)$$

The double volume and double surface integrations in (4) and (5) are performed in cell coordinates of the corresponding hexahedral or quadrilateral PEEC cells and the free space Green's function is used

$$G(\mathbf{r}, \mathbf{r}') = \frac{e^{-jk|\mathbf{r}-\mathbf{r}'|}}{4\pi|\mathbf{r}-\mathbf{r}'|} \approx \frac{1}{4\pi|\mathbf{r}-\mathbf{r}'|}, \quad (6)$$

where, throughout the remainder of this paper, the time retardation is neglected.

III. NON-ORTHOGONAL PARTIAL ELEMENT CALCULATION USING ANALYTIC FILAMENT FORMULAS

In the case where non-orthogonal PEEC cells are present and where no analytic expressions for the partial element

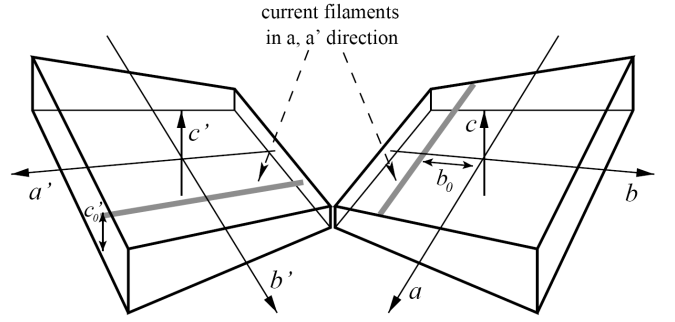


Figure 2. Two inductive hexahedral PEEC volume cells with current direction a and a' . The coordinate axes indicate a local non-orthogonal coordinate system, as introduced in [4]. Furthermore, two current filaments, pointing respectively in a and a' direction, are displayed.

calculations exist, the numeric evaluation of (4) and (5) requires a huge computational effort due to the dimensional manifold and the fact that the Lp - and Pn -matrices are dense and full, respectively. In particular, the self terms on the matrix diagonals require special attention due to the singularity in Green's function (6). In the following, an efficient calculation method for the inductance matrix and coefficient of potential matrix fill-ins is derived, using analytic iteration formulas for the mutual inductance between arbitrarily aligned current filaments.

General Non-Orthogonal Inductance Calculation

Insertion of a four-fold δ -pulse function into the non-orthogonal Lp definition (4) gives a relation between the mutual inductance of infinitesimal thin current filaments and the non-orthogonal volume mutual inductance

$$Lp_{aa'} = \mu \iiint_a \iiint_b \iiint_{c'} \iiint_{a'} \iiint_{b'} \iiint_{c''} \delta(b - b_0, b' - b'_0, c - c_0, c' - c'_0) \dots \hat{\mathbf{a}}' \cdot \hat{\mathbf{a}} \left| \frac{\partial \mathbf{r}}{\partial a} \right| \left| \frac{\partial \mathbf{r}'}{\partial a'} \right| G(\mathbf{r}, \mathbf{r}') dv dv' \quad (7)$$

$$= Lp_{ff}(b_0, b'_0, c_0, c'_0).$$

The geometric proportions are exemplified in Fig 2. Taking into account the integration property of Dirac's $\delta(\cdot)$ pulse function¹ reduces the double volume integration (4) into a double surface integral. Therefore, one obtains a simplified expression for the partial mutual inductance between two non-orthogonal volume cells

$$Lp_{aa'} = \iiint_b \iiint_{b'} \iiint_{c'} Lp_{ff}(b, b', c, c') da da' db db'. \quad (8)$$

Hence, Lp in equation (4) can be expressed using only the integral of the analytic solution Lp_{ff} for mutual inductances between arbitrary aligned current filaments, which are well known [7], [8]

$$M = Lp_{ff}(R_1, R_2, R_3, R_4) = 2 \cos \epsilon \sum_{i=1}^4 c_i + \frac{\sum_{i=5}^8 c_i}{\sin \epsilon}. \quad (9)$$

The filament formula is a complicated expression including several hyperbolic and trigonometric functions c_i ,

¹ $\int \delta(x - x_0) f(x) dx = f(x_0)$

TABLE I
COEFFICIENTS FOR FILAMENT LP AND P-CALCULATIONS

i	c_i
1	$+(\mu + l) \tanh^{-1} \frac{m}{R_1 + R_2}$
2	$+(\nu + m) \tanh^{-1} \frac{l}{R_1 + R_4}$
3	$-\mu \tanh^{-1} \frac{m}{R_3 + R_4}$
4	$-\nu \tanh^{-1} \frac{l}{R_2 + R_3}$
5	$+\tanh^{-1} \frac{d^2 \cos \varepsilon + (\mu + l)(\nu + m) \sin^2 \varepsilon}{dR_1 \sin \varepsilon}$
6	$-\tanh^{-1} \frac{d^2 \cos \varepsilon + (\mu + l)\nu \sin^2 \varepsilon}{dR_2 \sin \varepsilon}$
7	$+\tanh^{-1} \frac{d^2 \cos \varepsilon + \mu\nu \sin^2 \varepsilon}{dR_3 \sin \varepsilon}$
8	$-\tanh^{-1} \frac{d^2 \cos \varepsilon + \mu(\nu + m) \sin^2 \varepsilon}{dR_4 \sin \varepsilon}$

which are summarized in Table 1 and the required length and angle parameters can be extracted from Fig. 3.

The inductance formula is analytically exact, however, care must be taken of its numerical evaluation. For some special geometric arrangements, the hyperbolic functions as well as the fractions in (9) and c_i diverge to infinity. For instance, this is the case when the filaments intersect, touch or when they are in parallel. Nevertheless, the analytical limit is always well defined, and the use of a series expansion is required to obtain accurate results when such a divergence is detected.

General Non-Orthogonal Coefficients of Potential Calculation

Similar to the shown inductance calculation, the partial coefficients of potential calculation (5) can be reduced to a double line integral. This is possible due to the mathematical similarity between equations (4) and (5). Therefore, (9) has to be adopted in the following way

$$P = P_{ff}(R_1, R_2, R_3, R_4) = \frac{1}{\mu_0 \varepsilon_0} \frac{1}{lm} \left(\sum_{i=1}^4 2c_i + \frac{\sum_{i=5}^8 c_i}{\sin \varepsilon} \right), \quad (10)$$

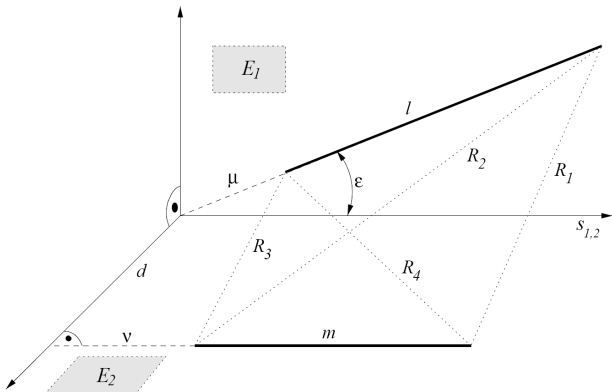


Figure 3. Shown are two arbitrarily aligned current filaments l and m and the required distances and angles for the mutual inductance calculation, see equations (9) and (10). Two Planes E_1 and E_2 are passed through the filaments in such a way as to intersect at right angles. Here, $s_{1,2}$ is the intersection line between the planes, having the filament m in parallel. The geometrical filament arrangement is completely determined by 6 independent parameters, e.g. $R_{1..4}$, m and l .

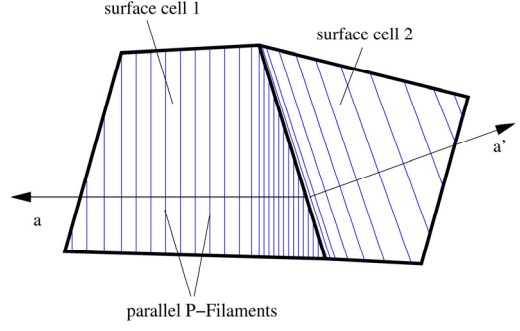


Figure 4. Two PEEC surface cells and the integration geometry for the coefficients of potential calculation are illustrated. Since the charge density has to be constant over every surface cell, the filaments have to be parallel, in contrast to the mutual inductance calculation, where the current density is varying inside a volume cell.

where the inner product of (8) was removed by omitting the $\cos(\varepsilon)$ term. Additionally, one has to take into account the electric field coupling constant and the fact that (5) has a lower dimension by dividing with the filament lengths l and m , the remainder of equation (9) is unchanged.

Furthermore, there is no charge density fluctuation over the integration surfaces of (5), in contrast to a variable volume current density in (4). This is an approximation due to the finite surface cell size and makes sense, since the node voltages, which determine the surface charge distribution [9], are not known a priori during matrix fill-in. This fact has to be considered during the reduced two-fold integration of

$$Pn_{aa'} = \iint_{a a'} P_{ff}(R_1, R_2, R_3, R_4) da da', \quad (11)$$

which is illustrated in Fig. 3. The corresponding surface charge filaments have to be parallel within the surface cell, whereas the integration direction (a, a') can be selected arbitrarily.

IV. EXTENSION TO CYLINDRICAL PEEC ELEMENTS

The partial element computation given above is generic and allows an extension of the standard PEEC method to different kinds of cell shapes, for instance cylindrical volume cells, which will be discussed here. For this kind of cell discretization, there are various application possibilities, for instance cable modeling, bond wires on discrete silicon devices, inductance balancing of power electronic modules, filter inductor modeling, printed circuit board vias or Rogowski coil modeling.

Standard PEEC models contain two distinct cell discretizations, volume current cells and surface charge cells which are shifted by half a discretization length, see Fig. 5. A similar discretization can be applied to cylindrical elements, where the volume between two nodes accounts for the inductive field coupling and the cylinder surface contains the corresponding surface charge elements, which are again shifted by half a discretization length. This approach can then be integrated seamlessly into the standard PEEC formulation. The major challenge for cylindrical cells is the computation of the partial element values. The most straightforward method in the sense of speed and accuracy is to use exclusively analytic formulas.

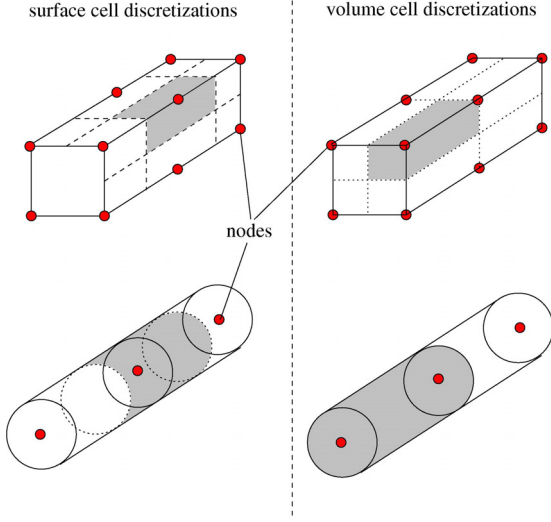


Figure 5. Discretization of PEEC cells. The left column shows the surface cell discretization and the right column the volume discretization, where one volume- and surface cell was shaded in gray, respectively. The discretization of cylindrical cells is performed similar to the conventional bars, where the surface elements are shifted by half a cell length.

However, such formulas are only available for the simplest geometry alignments, namely the self inductance and self coefficients of potential in the case of cylinder elements. The self inductance of a straight wire computes as

$$L_{ii} = 2 \cdot 10^{-11} l \left[\ln \left(\frac{l}{r} + \sqrt{1 + \left(\frac{l}{r} \right)^2} \right) - \sqrt{1 + \left(\frac{r}{l} \right)^2} + \frac{r}{l} + \frac{1}{4} \right],$$

where l is the wire length and r the radius the cylinder element. The self coefficient of potential can be calculated by a similar expression, obtained by integrating over the cylinder surface

$$P_{ii} = \frac{2 \cdot 10^{-11}}{\mu_0 \epsilon_0} \left[\ln \left(\frac{l}{r} + \sqrt{1 + \left(\frac{l}{r} \right)^2} \right) - \sqrt{1 + \left(\frac{r}{l} \right)^2} + \frac{r}{l} \right].$$

For the mutual (off-diagonal) matrix entries, no analytic solution is known, and therefore a numeric integration has to be applied. However, instead of using (2) and (3), the integration formalism derived in the previous section (9, 10) can be used to speed up the computation for cylindrical shaped PEEC cells. It is noteworthy that the equations apply not only to the magnetic and electric field couplings between distinct cylinder cells, but also between mixed elements, e.g. cylinders and conventional or non-orthogonal PEEC cell hexahedrals.

V. NUMERIC RESULTS AND VALIDATION

Despite the transcendent function evaluations, a numeric evaluation of (8) speeds up the integration. Besides the integration order reduction, the speedup is caused by a smoothing of the Green's function singularity (8), which is shown in Fig. 6. In particular, this smoothing property facilitates a fast calculation of the diagonal matrix entries, for which the volumes v and v' in (4) coincide.

The proposed accelerated partial element calculation was implemented in C++, using an adaptive integration routine based on a recursive Simpson algorithm with error estimation [10]. This gives the opportunity to select any

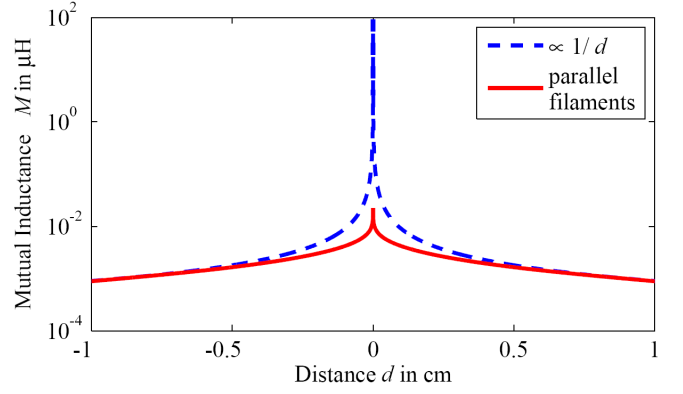


Figure 6. Mutual inductance between two parallel current filaments of length $l = 1$ cm. Approaching a zero distance d , the inductance M is diverging to infinity. However, the divergence $\log(2l/r)$ is relatively weak in comparison to the $1/d$ Green's function, which allows a more efficient numeric integration of the partial elements.

desired integration accuracy. Furthermore, the adaptive algorithm selects autonomously the number of interpolation points, which lowers the number of filament evaluations for inductive cells that are far apart, and refines the integration for adjacent cells or the self-terms.

A simple non-orthogonal application example

Fig. 7 shows an example of two inductive PEEC cells, for which the Lp calculation is investigated in the following. Cell 1 was chosen to be orthogonal. Therefore, an accurate reference value of L_{11} can be obtained from an analytic exact solution [11]. Cell 2 is a non-orthogonal hexahedral, hence for L_{12} and L_{22} , a numeric integration is mandatory. The proximity of cell 1 and 2 is a worst case for the mutual inductance calculation. Here, the recursive Simpson algorithm will increase the number of filament evaluations near the contact surface. The aspect ratio (length/thickness ≈ 10) of the shown cells is quite large. However, such thin and non-orthogonal structures are typical for many conductor geometries, e.g. [12] and [13].

To obtain another test case of mutual inductances, additionally to the main current direction in Fig. 4 (dashed), a second direction was introduced (dotted, corresponding Lp_{34}). The numeric inductance results are outlined in Table I for different integration resolutions. Here, the conventional Gauss-Legendre (GL) integration is directly applied to equation (4) and N gives the number of GL evaluation

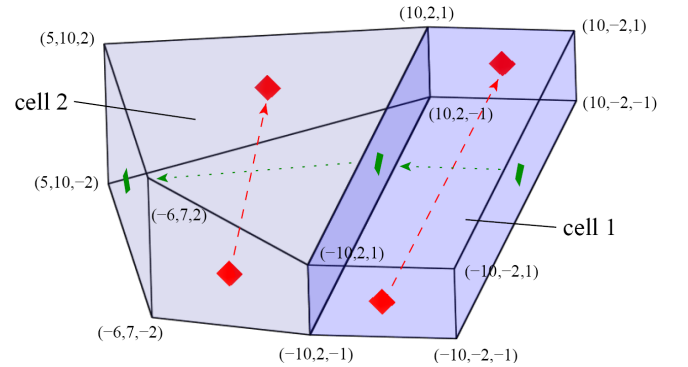


Figure 7. Example cell geometry: two inductive PEEC cells. Two different current directions (dashed and dotted) and the cell corner point coordinates are given (in mm) so that numeric results are replicable.

TABLE II
COMPARISON OF DIFFERENT INTEGRATION METHODS

	Lp_{11} [nH] N T [msec]	Lp_{22} [nH] N T [msec]	Lp_{12} [nH] N T [msec]	Lp_{34} [nH] N T [msec]
exact	9.8936	—	—	—
new filament integration algorithm	9.8934	5.70895	4.52591	0.364282
	9E6	9E6	2E5	2E5
	1E4	1E4	320	340
**	9.8921	5.70881	4.5260	0.36438
	1E5	1E5	14065	12889
	130	200	22	21
*	9.8958	5.71733	4.52618	0.369
	2401	2401	3277	2485
	2.7	3.9	5.2	4.1
conventional GL integration	9.58759	5.424	4.16366	0.3633
	2E6	2E6	2E6	2E6
	2000	2000	2000	2000
	9.4819	5.025	4.153	0.3625
	7E5	7E5	7E5	7E5
	600	600	600	600

TABLE I. Inductance values Lp_{ij} of the non-orthogonal cell geometry from Fig. 2, obtained from different integration routines and with varying numeric integration resolutions. Additionally, the number of integration steps N and the corresponding computation time T is given for every inductance value.

points [14]. In the case of the proposed filament algorithm using equation (8), N is the total number of filament evaluations. Furthermore, the total computation time on a 3 GHz CPU is given, respectively. Due to the singularity in the Green's function (6), GL integration consequently underestimates inductances. Even with fine resolution and hence with big numeric effort, the results do not have a satisfactory accuracy. In contrast, the new proposed method shows good convergence behaviour, which results in a more reasonable computation time. Obviously, the most time intensive computations are still performed for the matrix diagonal self-terms. Off-diagonal element computations need less computation time, which is further diminished with the increasing geometric cell distance.

For realistic problem sizes with e.g. $n=10^4$ non-orthogonal cells, the new method allows a Lp and Pn fill-in within 1 hour for **-accuracy in Table I, or about 10 minutes for *-accuracy, whereas GL integration would require orders of magnitudes more computation time.

Torroid inductor example

Fig. 8 shows two models of a torroid inductor, where the upper model consists of the previously introduced cylindrical cell shapes and the lower model is built from standard hexahedral cells. The size of the conventional inductor was chosen according to [15] with a cell width of $w = 1.745 r$, where r is the radius of the cylinder cells. With this choice, the self inductance and total inductance of both models should be roughly the same. For the reproducibility of the result, all dimensions are given in Fig. 8.

The impedance curves for both models is depicted in Fig. 9. As expected, the total low frequency inductance has no significant difference. However, resonance frequencies are significantly different, with an increasing deviation for

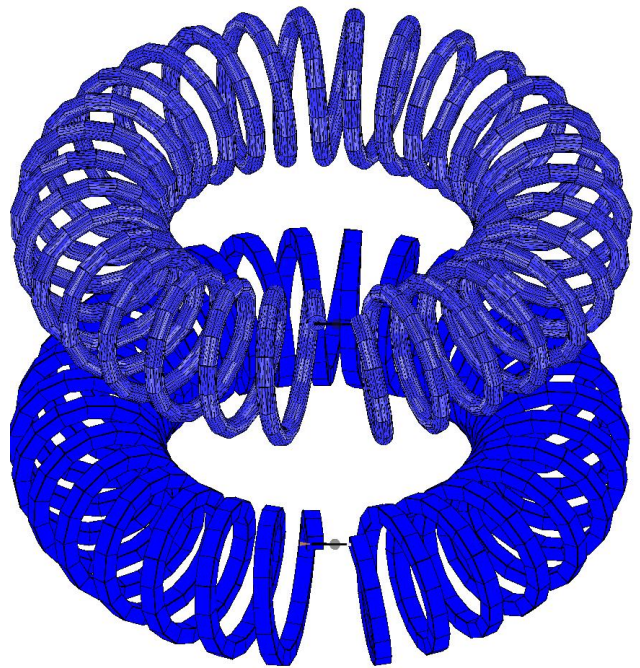


Figure 8. Two torroid inductors, built from cylindrical PEEC cells and conventional hexahedrals, respectively. Dimensions: 30 turns, torroid center radius 1cm, winding radius 0.03cm, wire radius $r = 0.04$ cm and $w = 0.07$ cm, respectively. Each inductor consists of 500 PEEC cells.

higher frequencies. This is reasonable, since the ratio per-length inductance and per-length capacitance is different for round and rectangular shaped wire. The main difference has its origin in the shape of electric field lines, which are converging at the presence of conductor edges.

A second issue is the computation speed for both models, which is more than an order of magnitude slower for the conventional model. For a correct modeling of the surface cell electric field properties, the hexahedral approach requires four nodes on the wire circumference, which increases the model size significantly.

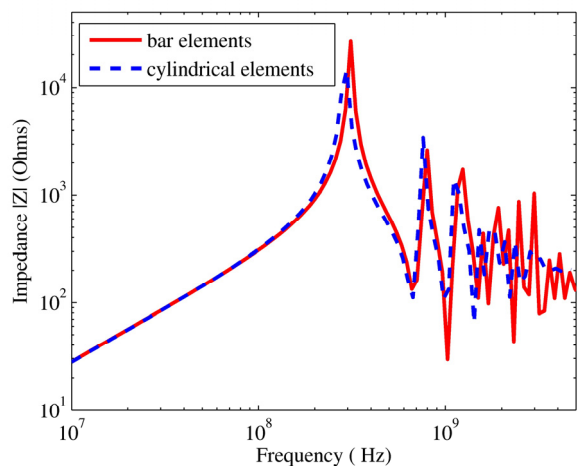


Figure 9. Impedance $|Z|$ of torroid inductors from Fig. 8. The total inductance is roughly the same, whereas first the resonance and especially the higher resonances differ significantly from each other.

VI. CONCLUSION AND OUTLOOK

This paper proposed a new numeric method for the evaluation of general non-orthogonal partial element matrix entries for PEEC simulations. With the usage of analytic mutual inductance formulas between arbitrary aligned current filaments, accuracy and speed of the partial element calculation is improved by orders of magnitudes in comparison to a conventional Gauss-Legendre integration routine. An analytic derivation of the proposed integration method was given and validated on an example cell geometry.

Additionally, the standard PEEC cell formulation was extended to cylindrical shaped cells, using the previously derived integration formalism. The simulation of a torroid inductor model with round wires shows reasonable results with good accuracy and improved simulation speed in comparison to a standard hexahedral cell approximation. A following step to this work will be an experimental verification of simulation results for cylinder cells with a comparison to experimental measurements.

A further extension of the proposed method for high frequency applications could be to take into account time retardation. In principle, a derivation of analytic filament formulas in [6] can be performed for a complex valued Green's function (6), resulting in complex L_p and P_n entries. This could be used to further improve time domain stability in comparison to the common used center-to-center retardation approximation [2].

REFERENCES

- [1] A. E. Ruehli, "Equivalent circuit models for three dimensional multiconductor systems," *IEEE Trans. on Microwave Theory and Techniques*, vol. 22, no. 3, pp. 216-221, 1974.
- [2] H. Heeb, A. E. Ruehli, "Retarded Models for PC Board Interconnects – Or How the Speed of Light Affects your SPICE Circuit Simulation," ICCAD, 1991.
- [3] A. E. Ruehli and H. Heeb, "Circuit models for three-dimensional geometries including dielectrics," *IEEE Trans. Microwave Theory Tech.*, vol. 40, no. 7, pp. 1507-1516, July 1992.
- [4] Ruehli, G. Antonini, J. Esch, J. Ekman, A. Mayo and A. Orlandi, "Nonorthogonal PEEC Formulation for Time- and Frequency-Domain EM and Circuit Modeling," *IEEE Transactions on Electromagnetic Compatibility*, vol. 45, no. 2, pp. 167-176, May 2003.
- [5] J. Ekman, G. Antonini, A. Orlandi and A. E. Ruehli, "Impact of Partial Element Accuracy on PEEC Model Stability," *IEEE Transactions on Electromagnetic Compatibility*, vol. 48, no. 1, pp. 19-31, February 2006.
- [6] F. F. Martens, "Über die gegenseitige Induktion und pondermotorische Kraft zwischen zwei stromdurchflossenen Rechtecken," *Ann. der Phys.*, vol. 343, no. 10, pp. 959-970, 1909.
- [7] F. W. Grover, "Inductance Calculations," *Dover Publications, Inc.*, New York, pp. 55-58, 1973.
- [8] G. A. Campbell, "Mutual Inductances of Circuits Composed of Straight Wires," *Phys. Review*, June 1915.
- [9] J. Ekman, G. Antonini, A. Orlandi, "3D PEEC capacitance calculations," *Int. Symp. on EMC*, vol. 2, pp. 630-635, 2003.
- [10] W. M. McKeeman, "Adaptive numerical integration by Simpson's rule, Algorithm 145," *Commun. ACM*, vol. 5, no. 12, pp. 604-605, 1962.
- [11] A. E. Ruehli, "Inductance Calculations in a Complex Integrated Circuit Environment," *IBM J. Res. Develop.*, vol. 22, no. 3, pp. 470-481, 1972.
- [12] M. Enohyaket and J. Ekman, "PEEC models for air-core reactors modeling skin and proximity effects" in *Proc. of Power Electronics Specialist Conference*, pp. 3034-3038, 2007.
- [13] A. Müsing, C. Zingerli and J. W. Kolar, "PEEC-Based Numerical Optimization of Compact Radial Position Sensors for Active Magnetic Bearings," *Proc. of 5th CIPS conference*, 2008.
- [14] G. Antonini, J. Ekman, A. C. Scogna, A. E. Ruehli, "A comparative study of PEEC circuit elements computation," *IEEE Int. Symp. on Electrom. Comp.*, vol. 2, pp. 810-813, 2003.
- [15] M. Paul, K. Roste, "Avoiding inductance problems," *Electronic Design*, vol. 25, 1974.